RESEARCH ARTICLE

Uhrf1 is indispensable for normal limb growth by regulating chondrocyte differentiation through specific gene expression

Michiko Yamashita[1,2], Kazuki Inoue[3], Noritaka Saeki[1,3], Maky Ideta-Otsuka[4], Yuta Yanagihara[1,3,6], Yuichiro Sawada[1,5], Iori Sakakibara[1,6], Jiwon Lee[7], Koichi Ichikawa[8], Yoshiaki Kamei[2], Tadahiro Iimura[7,9], Katsuhide Igarashi[4], Yasutsugu Takada[2] and Yuuki Imai[1,3,6,*]

ABSTRACT

Transcriptional regulation can be tightly orchestrated by epigenetic regulators. Among these, ubiquitin-like with PHD and RING finger domains 1 (Uhrf1) is reported to have diverse epigenetic functions, including regulation of DNA methylation. However, the physiological functions of Uhrf1 in skeletal tissues remain unclear. Here, we show that limb mesenchymal cell-specific Uhrf1 conditional knockout mice ($Uhrf1^{\Delta Limb/\Delta Limb}$) exhibit remarkably shortened long bones that have morphological deformities due to dysregulated chondrocyte differentiation and proliferation. RNA-seq performed on primary cultured chondrocytes obtained from $Uhrf1^{\Delta Limb/\Delta Limb}$ mice showed abnormal chondrocyte differentiation. In addition, integrative analyses using RNA-seq and MBD-seq revealed that Uhrf1 deficiency decreased genome-wide DNA methylation and increased gene expression through reduced DNA methylation in the promoter regions of 28 genes, including $Hspb1$, which is reported to be an IL1-related gene and to affect chondrocyte differentiation. $Hspb1$ knockdown in cKO chondrocytes can normalize abnormal expression of genes involved in chondrocyte differentiation, such as $Mmp13$. These results indicate that Uhrf1 governs cell type-specific transcriptional regulation by controlling the genome-wide DNA methylation status and regulating consequent cell differentiation and skeletal maturation.

KEY WORDS: Uhrf1, DNA methylation, Limb development, Chondrocyte differentiation, Hspb1

INTRODUCTION

Skeletal development and maturation are controlled by various transcription factors and growth hormone stimuli. During endochondral ossification in particular, condensed mesenchymal stem cells can commit to chondrocyte lineage cells and proliferate before terminally differentiating into hypertrophic chondrocytes (Kobayashi and Kronenberg, 2014). The failure of chondrocyte differentiation and maintenance can lead to pathological conditions such as osteoarthritis (Saito et al., 2010). Cell differentiation is governed by a network of transcription factors that promote continuous epigenetic effects such as DNA methylation, histone modification and chromatin remodeling (Bernstein et al., 2007; Li et al., 2007). Thus, an enhanced understanding of the mechanisms by which epigenetic regulators control complex physiological and pathological conditions can help elucidate disease pathology.

Ubiquitin-like with PHD and RING finger domains 1 (Uhrf1) acts as an epigenetic regulator, and its multiple functional domains maintain DNA methylation status by recognizing hemi-methylated DNA in divided nuclei (Bostick et al., 2007). Uhrf1 can bind to H3K9me2/3 via its PHD domain (Rajakumara et al., 2011) and ubiquitylate H3K23 residues (Nishiyama et al., 2013), which is followed by recruitment of Dnmt1 to hemi-methylated DNA (Liu et al., 2013). Uhrf1 is reported to play a role in development of several organs and physiological conditions, e.g. liver (Jacob et al., 2015), gut (Marjoram et al., 2015), brain (Murao et al., 2014) and immune responses (Obata et al., 2014). Moreover, Uhrf1 overexpression is associated with progression of various cancer types, including breast, pancreatic, bladder and colon (Abu-Alainin et al., 2016; Li et al., 2011; Sabatino et al., 2012; Yang et al., 2012); thus, Uhrf1 can serve as a molecular marker for these cancers (Geng et al., 2013; Unoki et al., 2009). DNA methylation in the promoter regions of various genes can be dysregulated by Uhrf1 overexpression and consequently cancer cell proliferation is facilitated. However, the function of $Uhrf1$ in skeletal tissue and limb development continues to be elusive. In this study, we sought to clarify the role of Uhrf1 in skeletal tissue using limb mesenchymal cell-specific $Uhrf1$ knockout mice.

RESULTS

$Uhrf1^{\Delta Limb/\Delta Limb}$ mice exhibit shortened limbs

To evaluate the significance of Uhrf1 function in skeletal growth and limb development, we generated limb mesenchymal cell-specific $Uhrf1$ conditional knockout mice (cKO; $Uhrf1^{\Delta Limb/\Delta Limb}$) by crossing $Prx1$-Cre and $Uhrf1$ floxed mice. Skeletal preparations from neonatal control mice and limb-specific Uhrf1 KO mice (cKO) showed that both genotypes had the expected bone and cartilage tissues, but cKO mice had slightly shorter limbs relative to control mice (Fig. 1A). Furthermore, cKO mice showed clavicular deformities and poor calcification in the phalangeal bones (Fig. 1B). To assess skeletal maturation in cKO mice, we next assessed long bone structures in 6-week-old mice by radiology. Micro-CT views of cKO femurs showed not only short limbs but also varus and torsional deformities (Fig. 1C), regardless of gender (Fig. S1A). The short length and morphological abnormalities in the limbs of cKO mice became more severe as the animals reached young adulthood (6 weeks of age). In particular, the shortening of

[1]Division of Integrative Pathophysiology, Proteo-Science Center, Ehime University, Toon, Ehime 791-0295, Japan. [2]Department of Hepato-Biliary-Pancreatic Surgery and Breast Surgery, Ehime University Graduate School of Medicine, Toon, Ehime 791-0295, Japan. [3]Division of Laboratory Animal Research, Advanced Research Support Center, Ehime University, Toon, Ehime 791-0295, Japan. [4]Life Science Tokyo Advanced Research center (L-StaR), Hoshi University School of Pharmacy and Pharmaceutical Science, Shinagawa-ku, Tokyo 142-8501, Japan. [5]Department of Urology, Ehime University Graduate School of Medicine, Toon, Ehime 791-0295, Japan. [6]Department of Integrative Pathophysiology, Ehime University Graduate School of Medicine, Toon, Ehime 791-0295, Japan. [7]Division of Bio-Imaging, Proteo-Science Center, Ehime University, Toon, Ehime 791-0295, Japan. [8]Department of Orthopaedic Surgery, Osaka City University Graduate School of Medicine, Osaka 545-8585, Japan. [9]Division of Analytical Bio-Medicine, Advanced Research Support Center, Ehime University, Toon, Ehime 791-0295, Japan.

*Author for correspondence (y-imai@m.ehime-u.ac.jp)
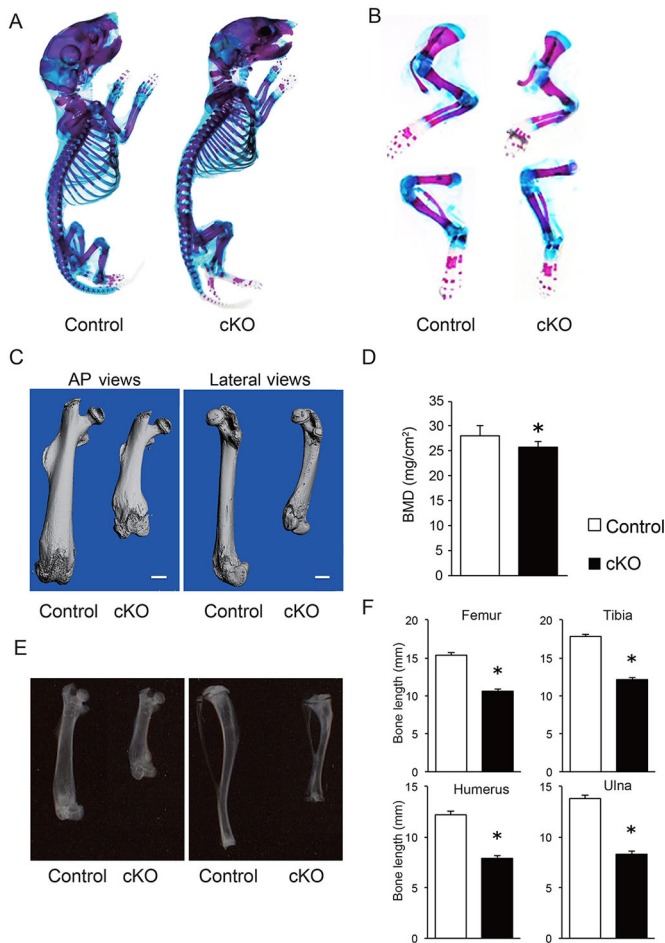
Y.I., 0000-0002-6119-0034

DEVELOPMENT

Fig. 1. Skeletal phenotypes in limb-specific *Uhrf1* KO mice. (A) Skeletal preparations (Alcian Blue/Alizarin Red) of neonatal control and limb-specific *Uhrf1* KO mice (cKO). Representative data from at least three individual mice are shown. (B) Higher magnification of skeletal preparation for forelimbs (upper panels) and hindlimbs (lower panels). Representative data from at least three individual mice are shown. (C) Micro CT views of femurs from 6-week-old male control and cKO mice. Scale bars: 1 mm. Representative data from at least three individual mice are shown. (D) Bone mineral density (BMD) of femurs from 6-week-old male control (n=8) and cKO (n=5) mice. (E) Representative soft X-ray of a femur and tibia from 6-week-old male control and cKO mice. Representative data from at least three individual mice are shown. (F) Quantitative data for Fig. 1E control (n=8) and cKO (n=5). The long bone length was calculated from the soft X-rays. All data are mean±s.d. *P<0.05 (Student's *t*-test or Mann–Whitney *U*-test).

the long bones was more apparent up until the age of 10 weeks (Fig. S1B). Furthermore, dual-energy x-ray absorptiometry (DXA) showed that femoral bone mineral density (BMD) of cKO male mice was significantly lower (∼20%) than that of control mice (Fig. 1D). Soft X-rays highlighted both bone deformities and shortened bone length in cKO mice (Fig. 1E), and that the long bone length in cKO mice was significantly decreased by more than 30% relative to control mice (Fig. 1F). These data indicated that Uhrf1 could have a significant role in longitudinal bone growth and that Uhrf1 deficiency in mesenchymal stem cells can lead to shortened limbs and morphological abnormalities of bones, especially during skeletal maturation after birth. Based on the abnormal phenotypes of the cKO mice, we next investigated endochondral ossification in Uhrf1-deficient mice. Alcian Blue and Nuclear Red staining of the proximal humerus at postnatal day 7 depicted disturbances in the orderly columnar structures of chondrocytes in the growth plates

of cKO mice (Fig. 2A), and the area of proliferative cartilage was decreased despite comparable proliferative length (Fig. 2B). Meanwhile, immunohistochemistry (IHC) against type X collagen (Col10) revealed that the length of Col10-positive hypertrophic
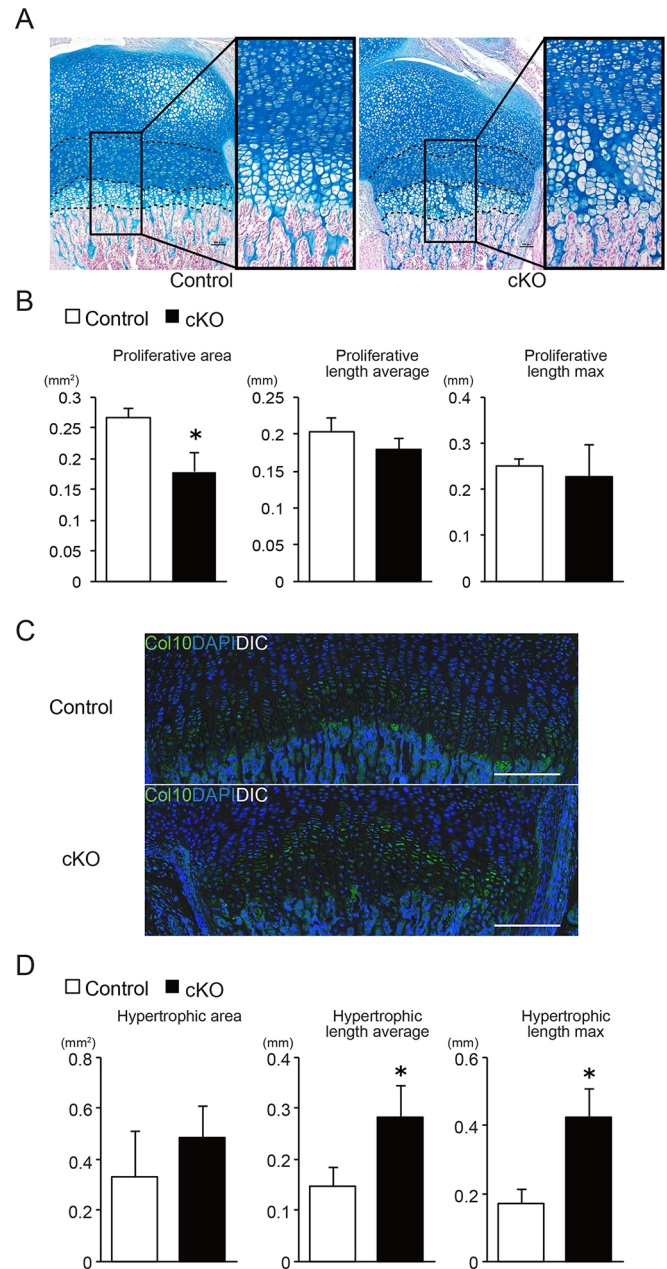

Fig. 2. Histological analyses for limb-specific *Uhrf1* KO mice. (A) Alcian Blue and Nuclear Red staining of the proximal humerus at postnatal day 7; right panels show higher magnifications of the boxed areas in the left panels. The broken lines indicate the boundary between the growth plate zones. Representative data from at least three individual mice are shown. Scale bars: 100 μm. (B) The area and length of proliferative cartilage of control (n=3) and cKO (n=6) mice were measured for the region of interest (ROI) in the proximal humerus, which was separated into 10 equal parts per animal, using ImageJ. (C) Immunohistochemistry against type X collagen (Col10, green) for the proximal humerus at postnatal day 7. Representative data from at least three individual mice are shown. Scale bars: 200 μm. (D) The area and length of hypertrophic cartilage of control (n=4) and cKO (n=4) mice were measured, according to Col10-positive staining in C. All data are mean±s.d. *P<0.05 (Student's *t*-test or Mann–Whitney *U*-test).

cartilage was increased in cKO mice (Fig. 2C,D). In addition, the growth plate disturbance was not normalized in 6-week-old cKO mice and the formation of the secondary ossification center was remarkably delayed (Fig. S2A), with hypertrophic chondrocytes in epiphysis. On the other hand, the morphology of osteoblasts (Fig. S2B) and osteoclasts (Fig. S2C) on bone surfaces of cKO mice was indistinguishable from that of control mice, although cortical bones of cKO mice showed woven bone-like histology. These results suggested that abnormal limb morphological phenotypes in $Uhrf1^{\Delta Limb/\Delta Limb}$ mice might be caused by dysregulated chondrocyte differentiation.

Uhrf1 deficiency disturbs chondrocyte differentiation

To investigate the cause of impaired chondrocyte differentiation, we evaluated primary chondrocyte cultures obtained from both control and cKO mice on neonatal day 3. $Uhrf1$ mRNA expression levels in cKO chondrocytes were significantly decreased (Fig. 3A) and Uhrf1 protein levels were also reduced to below the limit of detection (Fig. 3B). These results show that the Prx1-Cre-mediated conditional knockout of $Uhrf1$ successfully reduced Uhrf1 expression in chondrocytes. As Uhrf1 reportedly regulates cancer cell proliferation, we also assessed cKO cell proliferation activity by an MTT assay. Proliferation of chondrocytes from cKO mice was
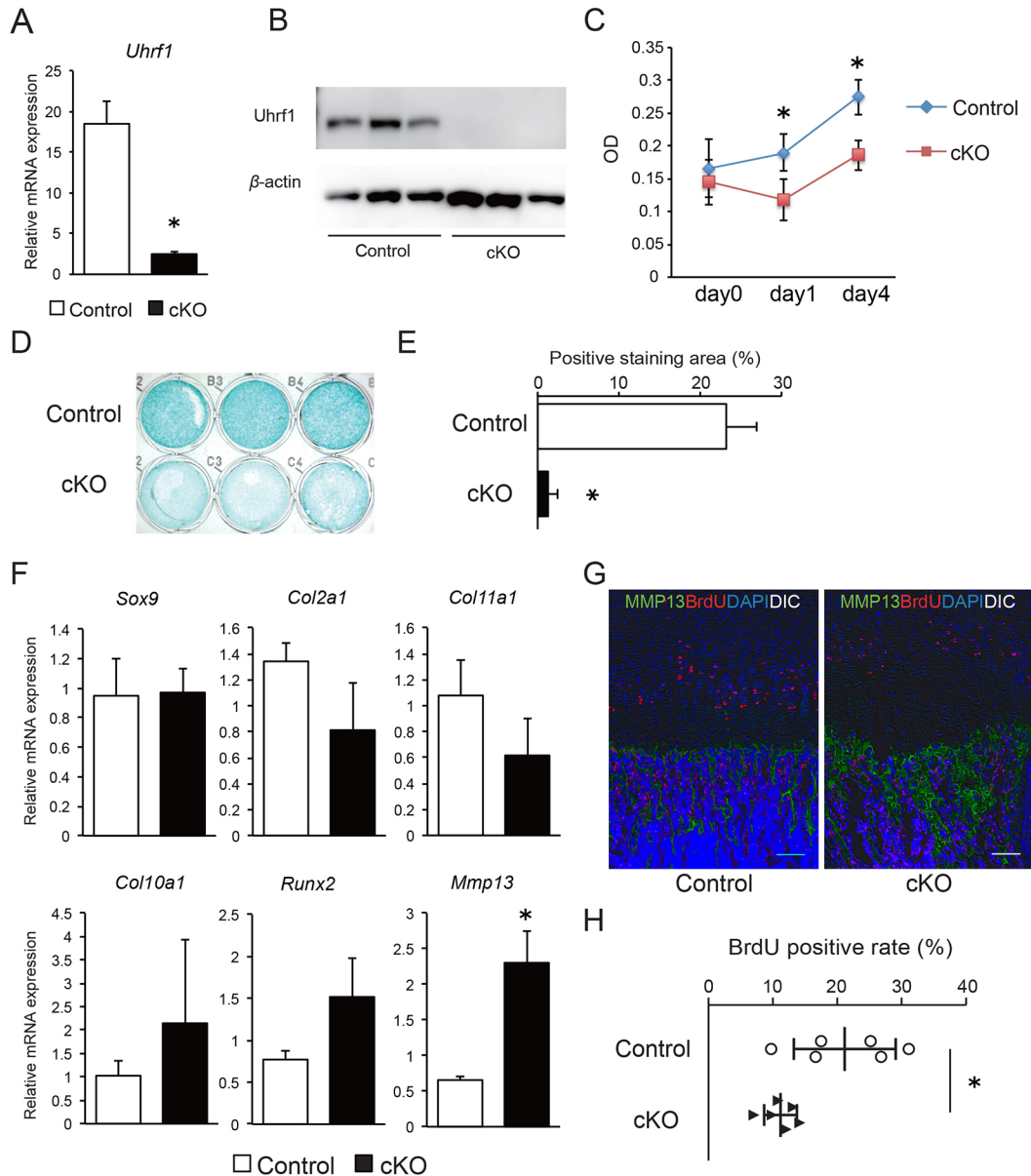

Fig. 3. _Uhrf1_-deficient chondrocytes exhibit abnormal cell proliferation and differentiation. (A) _Uhrf1_ mRNA expression levels in primary chondrocytes isolated from neonatal control and cKO mice (n=3). (B) Western blot analysis of Uhrf1 protein expression (n=3). (C) Cell proliferation of primary cultured chondrocytes obtained from control and cKO mice as determined by MTT assay (n=3). (D) Cartilage matrix synthesis by primary cultured chondrocytes obtained from control and cKO mice was evaluated by Alcian Blue staining (n=3). (E) Quantitative analysis of Alcian Blue staining (n=3). (F) Real-time RT-PCR results for expression levels of chondrocyte differentiation marker genes (n=3). (G) Immunohistochemistry for Mmp13 (green), BrdU (Red) and DAPI (blue) on the proximal humeral growth plate at postnatal day 7 of control and cKO mice. Representative data from at least three individual mice are shown. Scale bars: 100 µm. (H) BrdU-positive rate in the proximal humeral proliferative chondrocytes calculated using anti-BrdU immunohistochemistry as shown in G (n=6). All data are mean±s.d. *P<0.05 (Student's t-test).

decreased relative to control mice (Fig. 3C), which is consistent with earlier reports (Murao et al., 2014). Furthermore, Alcian Blue staining showed that positive cartilage matrix synthesis in primary cultured chondrocytes from cKO mice was significantly decreased compared with that of control mice (Fig. 3D,E), suggesting that chondrocyte differentiation is impaired in cKO mice. These results indicated that Uhrf1 might regulate both cell proliferation and cell differentiation. To test the chondrocyte differentiation in cells obtained from cKO mice, real-time RT-PCR was performed to detect expression of chondrocyte differentiation marker genes. The expression levels of early chondrocyte differentiation marker genes such as *Col2a1* and *Col11a1* tended to be decreased, whereas expression of late marker genes, including *Col10a1* and *Runx2*, was increased in cKO cells. Among these marker genes, expression levels of *Mmp13* were also significantly elevated in cKO cells (Fig. 3F). In addition, immunohistochemistry to detect Mmp13 expression in the proximal humeral growth plate of postnatal day 7 mice displayed remarkably increased expression of Mmp13 protein in cKO mice relative to control mice, especially in the lower layer of the hypertrophic zone (Fig. 3G). Meanwhile, the frequency of proliferative chondrocytes that had positive BrdU staining was significantly decreased in cKO mice compared with control mice (Fig. 3G,H). These data suggested that Uhrf1 deficiency dysregulated both chondrocyte differentiation and proliferation due to an altered transcriptome profile arising from changes in Uhrf1-mediated DNA methylation.

Uhrf1 deficiency facilitates expression of gene sets

To identify gene expression profile changes in Uhrf1-deficient cells that might impair chondrocyte differentiation, we performed RNA-seq on primary cultured chondrocytes obtained from both control and cKO mice (Fig. 4A). Of the genes with expression levels that differed between cKO cells and control cells by more than twofold, 1137 and 1089 genes showed up- and downregulation, respectively. However, a Volcano plot clearly revealed that there were more upregulated genes (324 genes) than downregulated genes (98 genes) among the genes with significant ($P<0.05$) differential expression (Fig. 4B). Among the 324 genes that showed significant upregulation, only 13 genes (Table S1) overlapped with the 160 genes that showed upregulated expression in hematopoietic stem cells (HSC) lacking *Uhrf1* (Zhao et al., 2017) (Fig. 4C). These results indicated that Uhrf1 deficiency in chondrocytes could induce transcriptional upregulation of various chondrocyte-specific genes. To characterize these significantly differentially expressed genes, we performed Gene Ontology (GO) analyses using Database for DAVID bioinformatics resources (david.ncifcrf.gov). Functional annotation clustering of keywords such as glycoprotein, secreted and cell adhesion was detected among the GO terms (Fig. S3A). Among the upregulated genes, focal adhesion or cell-adhesion pathway (Fig. 4D) and biological process (Fig. S3B) were enriched in both categories. Gene set enrichment analysis (GSEA) also revealed that a focal adhesion gene set was significantly enriched among differentially expressed genes (Fig. S4A). To validate this observed enrichment in focal adhesion genes, we performed real time RT-PCR on the identified genes in cKO and control samples. In cKO chondrocytes, significant upregulation was validated for focal adhesion-related genes such as *Ibsp*, *Itga2*, *Itga11* and *Tnn*. Meanwhile, there were fewer adhesion-related genes with downregulated expression (Fig. S4B). These results suggested that increased expression of genes involved in focal adhesion pathways
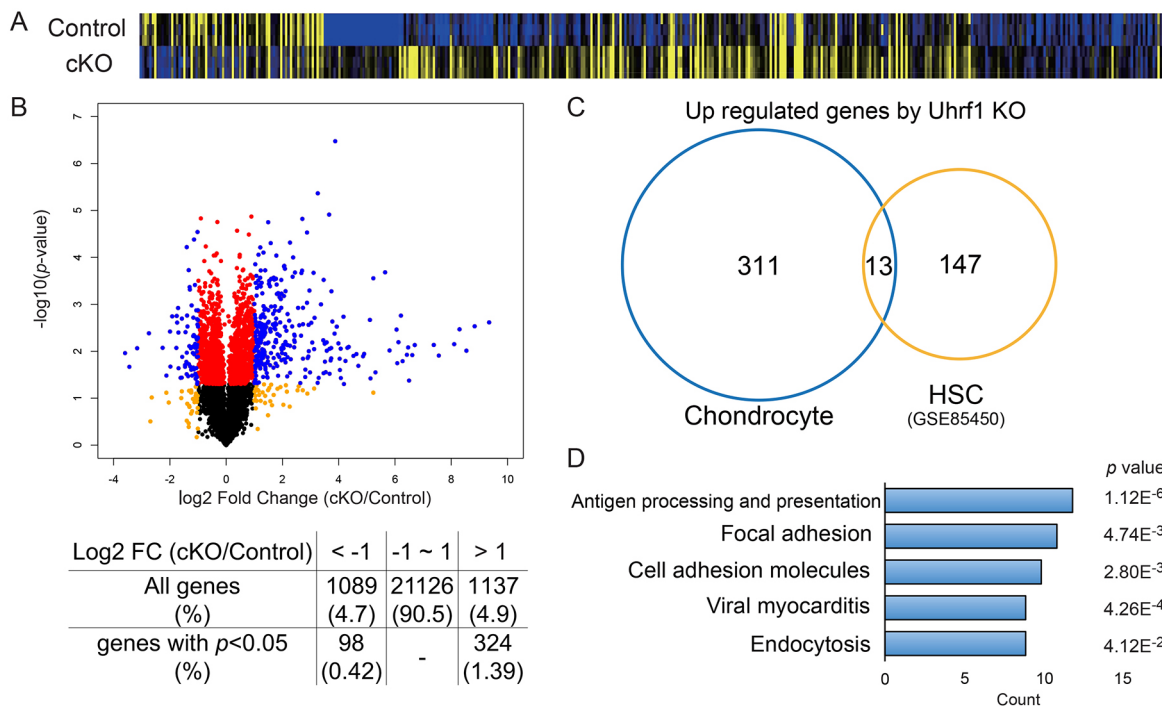

Log2 FC (cKO/Control)	< -1	-1 ~ 1	> 1
All genes	1089	21126	1137
(%)	(4.7)	(90.5)	(4.9)
genes with *p*<0.05	98	-	324
(%)	(0.42)		(1.39)

Fig. 4. RNA-sequence results from primary chondrocytes. (A) Heatmap (high, yellow; low, blue) and (B) Volcano plot for RNA-seq data obtained from primary cultured chondrocytes treated with rhBMP-2 for 1 day. Blue dots indicate genes that were significantly (*P*<0.05) and differentially expressed in cKO cells by more than twofold. The table summarizes the number and percentage of differentially expressed genes (upper row) and significantly expressed genes (lower row). (C) Venn diagram for the number of upregulated genes in the presence of Uhrf1 deficiency in chondrocyte and hematopoietic stem cells (HSCs) (taken from the dataset GSE85450). Thirteen genes overlapped between two data sets, which are listed in Table S1. (D) Gene Ontology (GO) analyses were performed using DAVID Bioinformatics Resources. The top five enriched GO KEGG pathways in the 324 upregulated genes are illustrated by gene counts and *P* values.

could affect chondrocyte differentiation or be subject to secondary transcriptional effects arising from the Uhrf1 deficiency.

Uhrf1 deficiency decreases DNA methylation and increases expression of specific genes

We next performed MBD2-mediated methylated DNA enrichment followed by next generation sequencing (MBD-seq) using primary chondrocytes obtained from control and cKO mice to clarify genome-wide changes in methylated DNA status caused by Uhrf1 deficiency and to analyze transcriptional regulation integratively. The amount of methylated DNA enriched in cKO cells was significantly lower than that in control cells (Fig. 5A). To identify Uhrf1-mediated methylated DNA loci, we performed peak calling by MACS2 using control cells as 'treatment' and cKO as 'control'. From these analyses, we successfully identified 35,861 Uhrf1-mediated peaks and these loci were significantly enriched in the gene body, promoter and downstream regions against genome

backgrounds (Fig. 5B). Although meta-gene analysis revealed that methylated DNA levels were high in the promoter region of all genes, methylation levels in the promoter region were higher in downregulated genes compared with upregulated genes (Fig. 5C). To identify Uhrf1 target genes in chondrocytes, we investigated which of the 324 upregulated genes in cKO mice overlapped with Uhrf1-mediated methylated DNA peaks. As a result, 28 genes with Uhrf1-mediated peaks in TSS (transcriptional start site)-3 kb (Fig. 5D and Table S2) were identified. Among these genes, we focused on *Hspb1* (heat shock protein β 1) and *Irak2* (interleukin 1 receptor-associated kinase 2), which were significantly highly expressed in cKO chondrocytes (Fig. 5E and Fig. S6A), because they are known to be related to IL1 signaling (Freshney et al., 1994; Hsu et al., 1995), which can facilitate *Mmp13* expression and cartilage degradation (Ahmad et al., 2007). Hspb1 expression was increased in the growth plate as well as in the primary spongiosa of cKO mice, as shown by IHC (Fig. 5G). We also focused on three
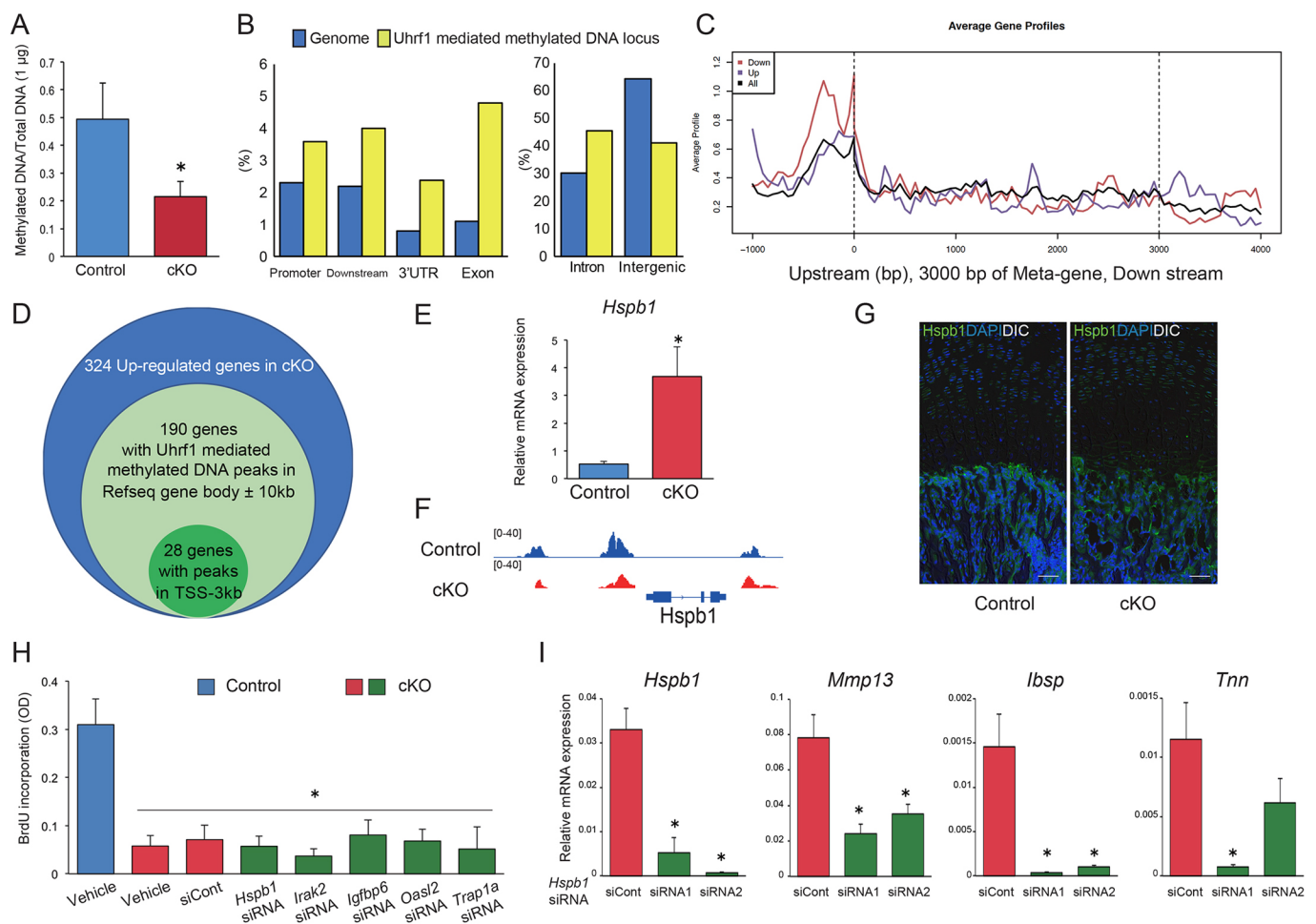

Fig. 5. Uhrf1-mediated DNA methylation governs chondrocyte differentiation. (A) The amount of MBD2-mediated enrichment in methylated DNA from 1 µg of total DNA obtained from control and cKO chondrocytes (*n*=3). (B) Distribution of Uhrf1-mediated methylated DNA that was annotated with the given intervals and scores with genome features by CEAS (cis-regulatory element annotation system). All differences were significant. (C) Meta-gene analysis of Uhrf1-mediated methylated DNA peaks. Peak signals on 'all genes' (black), 'down' (red) and 'up' (purple) regulated genes by Uhrf1 evaluated by RNA-seq results are described. (D) Venn diagram for the 324 upregulated genes in cKO (blue), 190 genes having Uhrf1-mediated methylated DNA peaks within the Refseq gene body ±10 kb (light green) and 28 genes with peaks in the promoter (3 kb) region (green), as listed in Table S2. (E) Real-time RT-PCR results for *Hspb1* expression in primary chondrocytes (*n*=3). (F) Methylated DNA signals around *Hspb1* genes (about 6 kb) illustrated by Igv (integrative genome viewer). (G) Immunohistochemistry for Hspb1 (green) and DAPI (blue) expressed at postnatal day 7 in the proximal humeral growth plate of control and cKO mice. Representative data from at least three individual mice are shown. Scale bars: 50 µm. (H) *In vitro* BrdU incorporation assay for primary cultured chondrocytes of control, cKO and cKO treated with siRNA for each gene (*n*=3). (I) Real-time RT-PCR results for cKO primary chondrocytes treated with rhBMP-2 for 3 days after siRNA for *Hspb1* treatment (*n*=3). All data are mean±s.d. *P<0.05 (Student's *t*-test, Mann–Whitney *U*-test or ANOVA).

genes, including *Igfbp6* (insulin-like growth factor binding protein 6), *Oasl2* (2′-5′ oligoadenylate synthetase-like 2) and *Trap1a* (tumor rejection antigen P1A), which were significantly highly expressed in cKO chondrocytes (Fig. S6A), because these genes were among the 13 genes that were upregulated in both chondrocytes and HSC (Fig. 4C and Table S1) with the 28 genes mentioned above (Fig. 5D and Table S2). In the promoter regions of *Hspb1* (Fig. 5F), *Irak2*, *Igfbp6*, *Oasl2* and *Trap1a* (Fig. S5A), levels of methylated DNA were reduced in cKO compared with the control. On the other hand, there was no significant change in methylated DNA levels in the promoter regions of *Mmp13*, *Tnn* and *Ibsp* (Fig. S7A), which all showed increased expression in cKO chondrocytes (Fig. 3F and Fig. S4B). These results indicated that Uhrf1 deficiency could broadly affect the expression of various genes and chondrocyte differentiation with or without direct alteration of methylated DNA levels. Finally, to validate the effects of increased expression of five genes (*Hspb1*, *Irak2*, *Igfbp6*, *Oasl2* and *Trap1a*) caused by Uhrf1 knockout on chondrocyte proliferation and differentiation, siRNA experiments for these five genes were performed using cKO chondrocytes (Fig. 5I and Fig. S6B). siRNA-knockdown of expression of these five genes could not rescue decreased chondrocyte proliferation, as evaluated by BrdU incorporation (Fig. 5H). However, siRNA for *Hspb1* could significantly suppress and normalize elevated expression of *Mmp13*, *Tnn* and *Ibsp* genes in cKO cells (Fig. 5I), whereas siRNA for the other four genes could not (Fig. S7B,C). Furthermore, siRNA for the overlapping three genes did not affect *Hspb1* expression levels (Fig. S7C), suggesting that high *Hspb1* expression was not secondary to the increased expression of the three genes. These results indicated that Uhrf1-mediated DNA methylation can orchestrate specific transcriptional expression networks, as well as consequent proliferation and differentiation. Moreover, these findings support that the defects in chondrocyte differentiation seen in cKO are, at least in part, due to the elevation in *Hspb1* expression that arises from Uhrf1 deficiency.

DISCUSSION
Uhrf1 is known to be a key molecule for the maintenance of DNA methylation, and its role in cell proliferation is important for progression of some cancers. However, the functional role of Uhrf1 in other processes, such as limb development, is unknown. In this study, we generated limb mesenchymal cell-specific Uhrf1 knockout mice (*Uhrf1*$^{\Delta Limb/\Delta Limb}$, cKO). The cKO mice had short and deformed limbs caused by growth plate irregularities. Given the ability of Uhrf1 to regulate cell proliferation, the reduced chondrocyte proliferation seen in cKO mice was expected. Chondrocytes lacking Uhrf1 exhibited not only impaired cell proliferation but also cell differentiation, which implies that Uhrf1 could also have a role in differentiation. *In vitro* primary cultures revealed that cKO chondrocytes had decreased synthesis of extracellular matrix proteins such as Col2 (Fig. 3D) and increased expression of hypertrophic makers such as *Mmp13* (Fig. 3F). These results indicate that cKO chondrocyte differentiation might be accelerated by Uhrf1 deficiency. This possibility is consistent with the increased hypertrophic zone length in cKO mice (Fig. 2C), but not with the hypertrophic area, which is a square measure affected by long bone size. In addition, these abnormal phenotypes in cartilage zones did not normalize over time, but instead the limb shortening and abnormal growth plate phenotypes worsened in adulthood (Figs S1B and S2A). These results indicated that Uhrf1-mediated chondrocyte differentiation as well as proliferation might be involved in the effects of growth hormones.

Several groups have proposed that Uhrf1 could have additional functions. Indeed, Obata et al. reported that mouse intestinal regulatory T cells lacking Uhrf1 showed defective proliferation and maturation with epigenetic impairment (Obata et al., 2014). Marjoram et al. reported that zebrafish harboring loss-of-function mutations in Uhrf1 exhibited intestinal inflammation due to TNFα overexpression that likely occurred in response to decreased DNA methylation of the TNFα gene promoter region (Marjoram et al., 2015). These previous reports indicate that Uhrf1 deficiencies could affect the epigenetic status of target genes and induce consequent transcriptomic changes during chondrocyte differentiation in *Uhrf1*$^{\Delta Limb/\Delta Limb}$ mice. Uhrf1 is known to have epigenetic effects associated with maintaining DNA methylation through the recruitment of DNA methyltransferase 1 (Dnmt1) and control of cell proliferation. However, recent results, including those in this study, revealed that Uhrf1 can also function in differentiating cells. These findings suggest that Uhrf1 might regulate *de novo* DNA methylation as well as maintenance DNA methylation. In fact, Meilinger et al. reported that Uhrf1 could interact with the *de novo* DNA methyltransferases Dnmt3a and Dnmt3b (Meilinger et al., 2009), suggesting that Uhrf1 may regulate chondrocyte differentiation by coordinating the transcriptome at the level of DNA methylation. On the other hand, a loss-of-function mutation in the DNMT3A gene causes an overgrowth syndrome that is characterized by a distinctive facial deformity, tall stature and intellectual disability (Tatton-Brown et al., 2014). The characteristics of this syndrome are inconsistent with the phenotypes of the *Uhrf1*$^{\Delta Limb/\Delta Limb}$ mice, suggesting that the phenotypes caused by the loss of the Uhrf1 gene could be related to Dnmt1, Dnmt3b or unknown functions of Uhrf1 rather than of Dnmt3a. Determining whether mice that lack DNA methyltransferases such as Dnmt1, Dnmt3a and Dnmt3b in chondrocytes have similar phenotypes to *Uhrf1*$^{\Delta Limb/\Delta Limb}$ mice will be important.

From the GO analyses of the genes with increased expression in cKO primary chondrocytes, genes in antigen-processing and -presentation pathways were enriched with increased expression of major histocompatibility complex (MHC)-related genes (Fig. 4D). However, whether MHC expression and chondrocyte differentiation are related is unclear, and thus increased MHC expression in primary chondrocytes could be a consequence of impaired chondrocyte differentiation. Genes associated with viral myocarditis were also enriched (Fig. 4D), which is relevant to a recent report that demonstrated changes in immune response genes in *Uhrf1*-deficient zebrafish (Chernyavskaya et al., 2017) [correlating with our expression data (Fig. S3B)], and might be involved in upregulation of the identified target genes. On the other hand, one representative pathway, focal adhesion, was enriched in bioinformatic analyses of RNA-seq data from control and cKO chondrocytes. This result suggested that increased expression of genes related to focal adhesion pathways could affect chondrocyte differentiation. Consistent with these results, Shin et al. showed that increased expression levels of focal adhesion complexes might lead to chondrocyte de-differentiation, and a FAK inhibitor could induce chondrocyte differentiation even in primary chondrocytes with increased passage number (Shin et al., 2016).

In this study, integrative analyses using MBD-seq and RNA-seq could identify direct and specific target genes of Uhrf1 in chondrocytes, such as *Hspb1*. Hspb1 is a downstream factor in IL1 signaling and can increase *Mmp13* expression as well as induce articular cartilage degeneration (Ahmad et al., 2007; Freshney et al., 1994). Although there are differences between articular and growth plate chondrocytes, these reports help to elucidate Uhrf1 and Hspb1 functions in chondrocyte differentiation. In addition, *Hspb1*

overexpression impaired chondrocyte differentiation as well as cell adhesion (Favet et al., 2001), which were both dysregulated in chondrocytes lacking Uhrf1 (this study). Moreover, Hspb1 has recently been reported to suppress osteoblast function and activity (Kainuma et al., 2017; Kuroyanagi et al., 2015). Although osteoblasts in cKO mice appeared normal (Fig. S2B), these reports might explain the presence of decreased BMD in $Uhrf1^{\Delta Limb/\Delta Limb}$ mice that had increased Hspb1 expression in both osteoblasts and chondrocytes (Fig. 5G). Hspb1 knockdown by siRNA reduced abnormal Mmp13 expression in cKO chondrocytes (Fig. 5I) but failed to normalize reduced cell proliferation of cKO chondrocytes (Fig. 5H), suggesting that Uhrf1 has other target genes that could be involved in regulating cell proliferation. Taken together, results from previous reports and this study indicate that Uhrf1 deficiency can increase the expression of target genes such as Hspb1, and these genes can induce aberrant transcriptional regulation in chondrocytes and subsequent abnormal chondrocyte differentiation. However, as shown in Fig. 4C, only 4-8% of upregulated genes in chondrocytes and HSCs lacking Uhrf1 overlapped. These overlapping genes affected neither chondrocyte proliferation nor differentiation, and also did not impact Hspb1 expression (Fig. 5H and Fig. S7C). This result indicates that Uhrf1 specifically regulates gene expression in chondrocytes, as shown in this study. As such, further study is needed to elucidate cell type-specific regulation of DNA methylation mediated by Uhrf1. In conclusion, the epigenetic regulator Uhrf1 can modulate cell type specific transcriptional regulation through effects on genome-wide DNA methylation status and consequent cell differentiation and skeletal maturation.

MATERIALS AND METHODS
Animals
Uhrf1 mutant knockout-first mice ($B6Dnk;B6N-Uhrf1^{<tm1a(EUCOMM)Wtsi>}/Ieg$) were obtained from The European Mouse Mutant Archive (EMMA) (Skarnes et al., 2011) and floxed mice were generated by crossing with ACTB-Flpe mice (Jackson Laboratory). $Uhrf1^{flox/flox}$ mice were crossed with Prx1Cre mice [B6.Cg-Tg(Prrx1-cre)1Cjt/J, Jackson Laboratory] to generate Prx1Cre; $Uhrf1^{flox/+}$ mice; Prx1Cre; $Uhrf1^{flox/flox}$ ($Uhrf1^{\Delta Limb/\Delta Limb}$) mice were obtained by crossing male Prx1Cre; $Uhrf1^{flox/+}$ and female $Uhrf1^{flox/flox}$. $Uhrf1^{\Delta Limb/\Delta Limb}$ and $Uhrf1^{flox/flox}$ mice were considered as conditional knockout mice (cKO) and control mice (control), respectively. All mice were housed in a specific pathogen-free facility under climate-controlled conditions with a 12-h light/dark cycle, and were provided with water and standard diet (MF, Oriental Yeast, Japan) ad libitum. All animals were maintained and used according to the protocol approved by the Animal Experiment Committee of Ehime University, Japan.

Radiological examination
Long bones were harvested from 6- or 10-week-old littermates, fixed with 4% paraformaldehyde (PFA) for 1 day and soaked in 70% ethanol. Soft X-rays were obtained with a soft x-ray apparatus (Sofron). The BMD of femurs was measured by dual-energy X-ray absorptiometry (DXA) using a bone mineral analyzer (DCS-600EX, ALOKA). Micro computed tomography scanning of femurs was performed using a Scanco Medical μCT35 System (SCANCO Medical).

Skeletal preparation
Neonates were skinned, eviscerated and fixed in 100% ethanol for 24 h, before transfer into 100% acetone for 24 h. Skeletal samples were stained with 0.8% Alcian Blue followed by 0.1% Alizarin Red and 0.3% glacial acid dissolved in 70% ethanol for 4 days before sequential clearance in 1% KOH with glycerol. Cartilage and mineralized bone were stained blue and red, respectively.

Histology
At 7 days, 6 weeks and 10 weeks after birth, mice were euthanized and the limbs were removed for fixation with 4% PFA in PBS overnight at 4°C,

followed by decalcification with EDTA. For in vivo BrdU incorporation assays, 100 mg/kg of BrdU (Abcam: ab142567) was intraperitoneally injected on postnatal day 6, 24 h before euthanasia. Long bone samples were embedded in paraffin wax after dehydration and the paraffin sections were cut with a microtome (RM2255, Leica Biosystems) into 5 μm slices. Sections were prepared for Alcian Blue and Nuclear Red staining, tartrate resistant acid phosphatase (TRAP) staining (TRAP staining kit, Wako), Toluidine Blue (TB) staining (Sigma-Aldrich, 0.05%) and immunohistochemistry (IHC). IHC was performed by incubating rabbit anti-Col10 polyclonal antibody (LSL, LB-0092, 1:500), rabbit anti-Mmp13 polyclonal antibody (Abcam, ab39012, 1:100), rat anti-BrdU monoclonal antibody (Abcam, ab6326, 1:100) and rabbit anti-Hspb1 polyclonal antibody (Abcam, ab5579, 1:100) as primary antibodies overnight at 4°C. Specimens were then treated with DAPI (Sigma, D9542, 5 μg/ml) and the secondary antibodies Alexa fluor 488 goat anti-rabbit IgG (Life Technologies, A11008) and Alexa fluor 555 goat anti-mouse IgG (Life Technologies, A21422) for 1 h at room temperature. Specimen images were captured as previously described (Lee et al., 2014). Briefly, bright-field images with differential interference contrast were acquired using an upright microscopy system (Nikon ECLIPSE Ti), and image processing was conducted using NISE elements (Nikon). The area and distance of proliferative and hypertrophic cartilage were measured for the region of interest (ROI) in the proximal humerus according to the cell morphology, extracellular matrix density and immune-positive staining for Col10, which was separated into 10 equal parts per animal using ImageJ. 'Length average' means the average calculated from 10 parts of an individual and 'Length max' is the maximum value among 10 parts of an individual.

Cell culture and reagents
Primary cultured chondrocytes were obtained from the knee of postnatal day 3 mice as previously described (Si et al., 2013). Briefly, harvested knees were treated with 0.3% collagenase D (Roche) in Dulbecco's Minimum Essential Medium (DMEM, Wako) for 1 h and then treated with fresh media containing collagenase overnight. Cells were cultured in MEM α (Gibco) supplemented with 10% fetal bovine serum (FBS, Nichirei Biosciences) and 1% antibiotic/antimycotic solution (Gibco) at 37°C in an atmosphere of 5% CO_2. After the cells reached confluence, they were treated with 100 ng/ml recombinant human BMP2 (Osteopharma).

Alcian Blue staining
Primary chondrocytes were cultured with rhBMP2 (100 ng/ml) for 7 days and fixed with 4% PFA for 15 min. After washing with PBS twice, the fixed cells were rinsed with 0.1 N hydrochloric acid (HCl) solution for 5 min, stained with 1% Alcian Blue (Sigma-Aldrich) in 0.1 N HCl for 30 min, and then washed with 0.1 N HCl. The stained area was calculated using ImageJ. Each experiment was biologically replicated at least three times.

Real time RT-PCR
Total RNA was extracted with Trizol (Invitrogen) and an RNeasy spin column kit (QIAGEN), followed by treatment with DNase I (QIAGEN). First-strand cDNA was synthesized from total RNA using PrimeScript RT Master Mix (Takara Bio) and subjected to real time RT-PCR using SYBR Premix Ex Taq II (Takara Bio) with Thermal Cycler Dice (Takara Bio) according to the manufacturer's instructions. Gene expression levels were normalized relative to the expression level of the housekeeping gene Rplp0. Primer sequences are shown in Table S3. Each experiment was biologically replicated at least three times.

Western blotting
Primary culture cells were washed with PBS and dissolved in SDS buffer with protease and phosphatase inhibitors. Whole-cell extracts were separated by SDS-PAGE and transferred to polyvinylidene fluoride (PVDF) membranes. The membranes were blocked with 5% skim milk in PBS with Tween-20 (PBST). Anti-Uhrf1 antibody (H-8 200 μg/ml, F2911, Santa Cruz) or anti-β-actin antibody (1 μg/ml, 2F3, Wako) was bound overnight at 4°C. After washing with PBST, HRP-conjugated secondary antibody (1:1500, Dako) was bound for 1 h at room temperature.

Immunoreactive signals were detected using Chemi-Lumi One Ultra (Nacalai Tesque) and ImageQuant LAS 4000 (GE Healthcare). Each experiment was biologically replicated at least three times.

Cell proliferation assay
MTT [3-(4,5-dimethyl-2-thiazolyl)-2,5-diphenyltetrazolium bromide] assay kits (Nacalai Tesque) were used according to the manufacturer's instructions. Absorbance at 570 nm was measured using a microplate reader. Each experiment was biologically replicated at least three times.

In vitro BrdU proliferation assay
Cell proliferation analysis using BrdU incorporation was performed with a Cell Proliferation ELISA, BrdU kit (Roche: 1647229), according to the manufacturer's instructions. Briefly, 5×10^3 cells were plated in each well of a 96-well cell culture plate. The cells were cultured for 16 h and then treated with 100 ng/ml rhBMP2 for 24 h. Two hours after addition of BrdU, the cells were fixed and then incubated with POD-conjugated anti-BrdU antibody for 90 min. After washing with PBS, tetramethylbenzidine was added for 15 min. The absorbance was measured at 370 nm (reference wavelength: 492 nm) using an ELISA plate reader. Each experiment was biologically replicated at least three times.

siRNA
siRNA was purchased from Sigma-Aldrich and transfected into primary chondrocytes obtained from cKO mice using an electroporation apparatus (Neon, Invitrogen) as previously described (Inoue and Imai, 2014). After siRNA transfection, cells were treated with 100 ng/ml of rhBMP2 for 3 days and harvested for RNA extraction. Each experiment was biologically replicated at least three times.

RNA-seq
The integrity of isolated RNA was verified using an Agilent 2100 Bioanalyzer. RNA samples with an RNA integrity number (RIN) greater than eight were normalized to 100 ng/µl before further analyses. RNA-seq libraries were prepared using the Illumina TruSeq Stranded mRNA Sample Prep Kit setA according to the manufacturer's instructions and subsequently validated for an average size of about 330-340 bp using a 2100 Bioanalyzer and the Agilent DNA1000 kit. Sequencing of paired-end reads (75 bp) was performed with the MiSeq Reagent kit V3 150 cycle on a MiSeq system (Illumina). Sequence data were mapped on the mouse genome (mm10) using Tophat (Trapnell et al., 2009) and analyzed using Cufflinks (Trapnell et al., 2010).

MBD-seq
MBD-seq is an analytic tool for understanding genome-wide methylated and/or non-methylated DNA regions using methyl-CpG-binding domain protein 2 (MBD2), which can bind methylated CpG. Methylated DNA was enriched by MBD2-mediated precipitation and subjected to Next Generation sequencing. Highly methylated DNA regions were identified by sequence reads mapped on the reference genome. Extracted DNA from chondrocytes was sonicated with a Covaris sonicator to obtain ~300 bp fragments. MBD2-mediated enrichment of methylated DNA was performed using the methylated DNA enrichment kit EpiXplore (Takara Bio) according to the manufacturer's instructions. The amount of enriched methylated DNA from 1 µg total DNA was measured using Quantus Fluorometer (Promega). Enrichment of methylated DNA was confirmed by semi-quantitative PCR using primer pairs for DNA regions that were reported to be highly methylated in various tissues [Daz1 (Stelzer et al., 2015) and Zc3h13 (Hupkes et al., 2011)]. Primer sequences are as follows: Daz1 Fw, ACGGTGCTCAGAGTTCTGTC; Daz1 RV, CGGACTCAAC-CTTCTCAATG; and Zc3h13 FW, GGGATGTCCATGACTACAGGGAC; Zc3h13 RV, TCTCAGGTGGTTTCTGCCATAACTG. Libraries for MBD-seq analysis were prepared using the DNA SMART ChIP-Seq Kit (Takara Bio) according to the manufacturer's instructions and validated for an average size of about 300-700 bp using a TapeStation and the Agilent High Sensitivity D1000 ScreenTape kit. Each experiment was biologically replicated at least three times. Sequencing of paired-end reads (75 bp) was performed using the MiSeq Reagent kit V3 150 cycle on a MiSeq system

(Illumina) and mapped on the mouse genome (mm10) using CLC Genomics Workbench (QIAGEN).

Analysis of sequencing data
For RNA-seq, differentially expressed genes, which have expression levels that were significantly increased or decreased in cKO by more/less than twice/half that of control, were extracted for further analyses. A heatmap was generated using MeV (Howe et al., 2011) and Gene Ontology analyses were performed DAVID Bioinformatics Resources 6.7 (Huang et al., 2009) and Gene Set Enrichment Analysis (GSEA) (Subramanian et al., 2005) . For MBD-seq, peak calling was performed by MACS2 (Zhang et al., 2008) and integrative analyses were carried out using the Cistrome Analysis Pipeline (http://cistrome.org/ap/) as previously described (Inoue and Imai, 2014).

Statistical analysis
Sample sizes were not based on power calculations. No animals were excluded from analyses. We used a two-tailed unpaired Student's t-test to analyze differences between two groups with Microsoft Excel or EZR version 1.35 (Kanda, 2013). The normality of the two data sets was evaluated using a Kolmogorov–Smirnov test and a Shapiro–Wilk test at a significance level of 0.05. When the normality was or was not confirmed in the groups, two-tailed Student's t-test or Mann–Whitney U-test, respectively, was applied. In this study, a Mann–Whitney U-test was used for analysis of data presented in Figs 1F, 2B and 5A. ANOVA followed by post hoc Tukey's test was applied for multiple groups comparison using SPSS (IBM). For all graphs, data are represented as the mean±s.d. Statistical significance was accepted when $P<0.05$.

Author contributions
Conceptualization: M.Y., K. Inoue, Y.I.; Methodology: K. Inoue, I.S., K. Igarashi; Validation: N.S.; Formal analysis: Y.I.; Investigation: M.Y., N.S., M.I.-O., Y.Y., Y.S., J.L., K. Ichikawa, T.I., K. Igarashi, Y.I.; Data curation: Y.I.; Writing - original draft: M.Y., Y.I.; Writing - review & editing: T.I., K. Igarashi, Y.I.; Visualization: Y.I.; Supervision: Y.K., Y.T.; Funding acquisition: Y.I.

Data availability
Data sets from RNA-seq and MBD-seq have been deposited in the NCBI Gene Expression Omnibus with accession numbers GSE92641 and GSE99335, respectively.

Supplementary information
Supplementary information available online at
http://dev.biologists.org/lookup/doi/10.1242/dev.157412.supplemental

References
Abu-Alainin, W., Gana, T., Liloglou, T., Olayanju, A., Barrera, L. N., Ferguson, R., Campbell, F., Andrews, T., Goldring, C., Kitteringham, N. et al. (2016). UHRF1 regulation of the Keap1-Nrf2 pathway in pancreatic cancer contributes to oncogenesis. J. Pathol. 238, 423-433.
Ahmad, R., Qureshi, H. Y., El Mabrouk, M., Sylvester, J., Ahmad, M. and Zafarullah, M. (2007). Inhibition of interleukin 1-induced matrix metalloproteinase 13 expression in human chondrocytes by interferon gamma. Ann. Rheum. Dis. 66, 782-789.
Bernstein, B. E., Meissner, A. and Lander, E. S. (2007). The mammalian epigenome. Cell 128, 669-681.

DEVELOPMENT

Bostick, M., Kim, J. K., Esteve, P.-O., Clark, A., Pradhan, S. and Jacobsen, S. E. (2007). UHRF1 plays a role in maintaining DNA methylation in mammalian cells. *Science* **317**, 1760-1764.

Chernyavskaya, Y., Mudbhary, R., Zhang, C., Tokarz, D., Jacob, V., Gopinath, S., Sun, X., Wang, S., Magnani, E., Madakashira, B. P. et al. (2017). Loss of DNA methylation in zebrafish embryos activates retrotransposons to trigger antiviral signaling. *Development* **144**, 2925-2939.

Favet, N., Duverger, O., Loones, M.-T., Poliard, A., Kellermann, O. and Morange, M. (2001). Overexpression of murine small heat shock protein HSP25 interferes with chondrocyte differentiation and decreases cell adhesion. *Cell Death Differ.* **8**, 603-613.

Freshney, N. W., Rawlinson, L., Guesdon, F., Jones, E., Cowley, S., Hsuan, J. and Saklatvala, J. (1994). Interleukin-1 activates a novel protein kinase cascade that results in the phosphorylation of Hsp27. *Cell* **78**, 1039-1049.

Geng, Y., Gao, Y., Ju, H. and Yan, F. (2013). Diagnostic and prognostic value of plasma and tissue ubiquitin-like, containing PHD and RING finger domains 1 in breast cancer patients. *Cancer Sci.* **104**, 194-199.

Howe, E. A., Sinha, R., Schlauch, D. and Quackenbush, J. (2011). RNA-Seq analysis in MeV. *Bioinformatics* **27**, 3209-3210.

Hsu, H., Xiong, J. and Goeddel, D. V. (1995). The TNF receptor 1-associated protein TRADD signals cell death and NF-kappa B activation. *Cell* **81**, 495-504.

Huang, D. W., Sherman, B. T. and Lempicki, R. A. (2009). Systematic and integrative analysis of large gene lists using DAVID bioinformatics resources. *Nat. Protoc.* **4**, 44-57.

Hupkes, M., van Someren, E. P., Middelkamp, S. H. A., Piek, E., van Zoelen, E. J. and Dechering, K. J. (2011). DNA methylation restricts spontaneous multi-lineage differentiation of mesenchymal progenitor cells, but is stable during growth factor-induced terminal differentiation. *Biochim. Biophys. Acta* **1813**, 839-849.

Inoue, K. and Imai, Y. (2014). Identification of novel transcription factors in osteoclast differentiation using genome-wide analysis of open chromatin determined by DNase-seq. *J. Bone Miner. Res.* **29**, 1823-1832.

Jacob, V., Chernyavskaya, Y., Chen, X., Tan, P. S., Kent, B., Hoshida, Y. and Sadler, K. C. (2015). DNA hypomethylation induces a DNA replication-associated cell cycle arrest to block hepatic outgrowth in uhrf1 mutant zebrafish embryos. *Development* **142**, 510-521.

Kainuma, S., Tokuda, H., Yamamoto, N., Kuroyanagi, G., Fujita, K., Kawabata, T., Sakai, G., Matsushima-Nishiwaki, R., Kozawa, O. and Otsuka, T. (2017). Heat shock protein 27 (HSPB1) suppresses the PDGF-BB-induced migration of osteoblasts. *Int. J. Mol. Med.* **40**, 1057-1066.

Kanda, Y. (2013). Investigation of the freely available easy-to-use software 'EZR' for medical statistics. *Bone Marrow. Transplant.* **48**, 452-458.

Kobayashi, T. and Kronenberg, H. M. (2014). Overview of skeletal development. *Methods Mol. Biol.* **1130**, 3-12.

Kuroyanagi, G., Tokuda, H., Yamamoto, N., Matsushima-Nishiwaki, R., Kozawa, O. and Otsuka, T. (2015). Unphosphorylated HSP27 (HSPB1) regulates the translation initiation process via a direct association with eIF4E in osteoblasts. *Int. J. Mol. Med.* **36**, 881-889.

Lee, J.-W., Yamaguchi, A. and Iimura, T. (2014). Functional heterogeneity of osteocytes in FGF23 production: the possible involvement of DMP1 as a direct negative regulator. *BoneKEy Rep.* **3**, 543.

Li, B., Carey, M. and Workman, J. L. (2007). The role of chromatin during transcription. *Cell* **128**, 707-719.

Li, X., Meng, Q., Rosen, E. M. and Fan, S. (2011). UHRF1 confers radioresistance to human breast cancer cells. *Int. J. Radiat. Biol.* **87**, 263-273.

Liu, X., Gao, Q., Li, P., Zhao, Q., Zhang, J., Li, J., Koseki, H. and Wong, J. (2013). UHRF1 targets DNMT1 for DNA methylation through cooperative binding of hemi-methylated DNA and methylated H3K9. *Nat. Commun.* **4**, 1563.

Marjoram, L., Alvers, A., Deerhake, M. E., Bagwell, J., Mankiewicz, J., Cocchiaro, J. L., Beerman, R. W., Willer, J., Sumigray, K. D., Katsanis, N. et al. (2015). Epigenetic control of intestinal barrier function and inflammation in zebrafish. *Proc. Natl. Acad. Sci. USA* **112**, 2770-2775.

Meilinger, D., Fellinger, K., Bultmann, S., Rothbauer, U., Bonapace, I. M., Klinkert, W. E. F., Spada, F. and Leonhardt, H. (2009). Np95 interacts with de novo DNA methyltransferases, Dnmt3a and Dnmt3b, and mediates epigenetic silencing of the viral CMV promoter in embryonic stem cells. *EMBO Rep.* **10**, 1259-1264.

Murao, N., Matsuda, T., Noguchi, H., Koseki, H., Namihira, M. and Nakashima, K. (2014). Characterization of Np95 expression in mouse brain from embryo to adult: A novel marker for proliferating neural stem/precursor cells. *Neurogenesis* **1**, e976026.

Nishiyama, A., Yamaguchi, L., Sharif, J., Johmura, Y., Kawamura, T., Nakanishi, K., Shimamura, S., Arita, K., Kodama, T., Ishikawa, F. et al. (2013). Uhrf1-dependent H3K23 ubiquitylation couples maintenance DNA methylation and replication. *Nature* **502**, 249-253.

Obata, Y., Furusawa, Y., Endo, T. A., Sharif, J., Takahashi, D., Atarashi, K., Nakayama, M., Onawa, S., Fujimura, Y., Takahashi, M. et al. (2014). The epigenetic regulator Uhrf1 facilitates the proliferation and maturation of colonic regulatory T cells. *Nat. Immunol.* **15**, 571-579.

Rajakumara, E., Wang, Z., Ma, H., Hu, L., Chen, H., Lin, Y., Guo, R., Wu, F., Li, H., Lan, F. et al. (2011). PHD finger recognition of unmodified histone H3R2 links UHRF1 to regulation of euchromatic gene expression. *Mol. Cell* **43**, 275-284.

Sabatino, L., Fucci, A., Pancione, M., Carafa, V., Nebbioso, A., Pistore, C., Babbio, F., Votino, C., Laudanna, C., Ceccarelli, M. et al. (2012). UHRF1 coordinates peroxisome proliferator activated receptor gamma (PPARG) epigenetic silencing and mediates colorectal cancer progression. *Oncogene* **31**, 5061-5072.

Saito, T., Fukai, A., Mabuchi, A., Ikeda, T., Yano, F., Ohba, S., Nishida, N., Akune, T., Yoshimura, N., Nakagawa, T. et al. (2010). Transcriptional regulation of endochondral ossification by HIF-2alpha during skeletal growth and osteoarthritis development. *Nat. Med.* **16**, 678-686.

Shin, H., Lee, M. N., Choung, J. S., Kim, S., Choi, B. H., Noh, M. and Shin, J. H. (2016). Focal adhesion assembly induces phenotypic changes and dedifferentiation in chondrocytes. *J. Cell. Physiol.* **231**, 1822-1831.

Si, Y., Inoue, K., Igarashi, K., Kanno, J. and Imai, Y. (2013). Autoimmune regulator, Aire, is a novel regulator of chondrocyte differentiation. *Biochem. Biophys. Res. Commun.* **437**, 579-584.

Skarnes, W. C., Rosen, B., West, A. P., Koutsourakis, M., Bushell, W., Iyer, V., Mujica, A. O., Thomas, M., Harrow, J., Cox, T. et al. (2011). A conditional knockout resource for the genome-wide study of mouse gene function. *Nature* **474**, 337-342.

Stelzer, Y., Shivalila, C. S., Soldner, F., Markoulaki, S. and Jaenisch, R. (2015). Tracing dynamic changes of DNA methylation at single-cell resolution. *Cell* **163**, 218-229.

Subramanian, A., Tamayo, P., Mootha, V. K., Mukherjee, S., Ebert, B. L., Gillette, M. A., Paulovich, A., Pomeroy, S. L., Golub, T. R., Lander, E. S. et al. (2005). Gene set enrichment analysis: a knowledge-based approach for interpreting genome-wide expression profiles. *Proc. Natl. Acad. Sci. USA* **102**, 15545-15550.

Tatton-Brown, K., Seal, S., Ruark, E., Harmer, J., Ramsay, E., Del Vecchio Duarte, S., Zachariou, A., Hanks, S., O'Brien, E., Aksglaede, L. et al. (2014). Mutations in the DNA methyltransferase gene DNMT3A cause an overgrowth syndrome with intellectual disability. *Nat. Genet.* **46**, 385-388.

Trapnell, C., Pachter, L. and Salzberg, S. L. (2009). TopHat: discovering splice junctions with RNA-Seq. *Bioinformatics* **25**, 1105-1111.

Trapnell, C., Williams, B. A., Pertea, G., Mortazavi, A., Kwan, G., van Baren, M. J., Salzberg, S. L., Wold, B. J. and Pachter, L. (2010). Transcript assembly and quantification by RNA-Seq reveals unannotated transcripts and isoform switching during cell differentiation. *Nat. Biotechnol.* **28**, 511-515.

Unoki, M., Kelly, J. D., Neal, D. E., Ponder, B. A. J., Nakamura, Y. and Hamamoto, R. (2009). UHRF1 is a novel molecular marker for diagnosis and the prognosis of bladder cancer. *Br. J. Cancer* **101**, 98-105.

Yang, G.-L., Zhang, L.-H., Bo, J.-J., Chen, H.-G., Cao, M., Liu, D.-M. and Huang, Y.-R. (2012). UHRF1 is associated with tumor recurrence in non-muscle-invasive bladder cancer. *Med. Oncol.* **29**, 842-847.

Zhang, Y., Liu, T., Meyer, C. A., Eeckhoute, J., Johnson, D. S., Bernstein, B. E., Nussbaum, C., Myers, R. M., Brown, M., Li, W. et al. (2008). Model-based analysis of ChIP-Seq (MACS). *Genome Biol.* **9**, R137.

Zhao, J., Chen, X., Song, G., Zhang, J., Liu, H. and Liu, X. (2017). Uhrf1 controls the self-renewal versus differentiation of hematopoietic stem cells by epigenetically regulating the cell-division modes. *Proc. Natl. Acad. Sci. USA* **114**, E142-E151.

DEVELOPMENT